Quantum size effect in two-photon excited luminescence from silver nanoparticles

Vladimir P. Drachev,[1] E. N. Khaliullin,[1] W. Kim,[2] F. Alzoubi,[2] S. G. Rautian,[3] V. P. Safonov,[3] R. L. Armstrong,[2] and Vladimir M. Shalaev[1]

[1]*School of Electrical and Computer Engineering, Purdue University, West Lafayette, Indiana 47907, USA*

[2]*Department of Physics, New Mexico State University, Las Cruces, New Mexico 88003, USA*

[3]*Institute of Automation and Electrometry, Novosibirsk 630090, Russia*

(Received 19 September 2003; published 26 January 2004)

A direct manifestation of electron energy quantization in metal nanoparticles is observed in two-photon excited luminescence. Experiments reveal the discrete spectra in broadband anti-Stokes photoluminescence from aggregates of silver colloid particles. A theory based on a spherical quantum-well model for metal nanoparticles is in good agreement with experimental observations.

DOI: 10.1103/PhysRevB.69.035318 PACS number(s): 78.67.Bf, 78.55.Hx

Recent progress in the fabrication of plasmonic nanomaterials and their high potential for various applications in photonics and surface-enhanced spectroscopy resulted in a growing interest in the fundamental physical properties of metal nanoparticles. Among such properties is the energy discretization of conduction electrons in metal quantum dots. The quantum-size effect in metal particles has been studied since the 1960s.[1–3] Kawabata and Kubo[1] and Gor'kov and Eliashberg[2] considered the specific heat and magnetic and electronic properties caused by the discrete electron energy states in small particles. The energy quantization effect in nonlinear optical phenomena in metal nanoparticles was studied by Hache *et al.*[4] and further developed by Rautian.[5]

Since the first theory for metal nanoparticles by Kawabata and Kubo[1] considerable efforts have been made to observe directly the discrete states in optical spectra of metal particles. However, to our best knowledge these discrete energy states so far have not been seen in optical experiments. This is in sharp contrast with semiconductor particles, where the quantum size effect is readily observed and has already found numerous applications, e.g., in quantum-well lasers. Such a striking difference results from the fact that metals, as opposed to semiconductors, do not have a finite energy gap between occupied and unoccupied electron states. As a result, the electron-hole interaction in metals is screened off and electrons behave as nearly free particles. So far experimental studies of various quantum-size effects in the optical properties were limited mainly to the size-dependence of the dielectric permittivity, $\epsilon=\epsilon_1+i\epsilon_2$, in small metal particles[3] (also see Refs. 6 and 7). The observed spectral width of the plasmon peak in absorption and its temperature dependence varies in accord with the (1/R)-law predicted for $\epsilon_2(R)$[1] and for $d\epsilon_2(R)/dT$.[8]

To observe the discrete character of closely spaced energy states in metal nanoparticle we employed resonant two-photon excited photoluminescence (PL). Note that in contrast to bulk metal, where luminescence is forbidden by the translation invariance, here it can occur in small nanoparticles.[9–11] Two-photon excited PL provides the spectral selectivity by ''choosing'' among many energy levels only those which are simultaneously in one- and two-photon resonances with the exciting light. These resonant levels give a much greater contribution to the nonlinear PL. Since there is a relatively small number of such ''double-resonant'' energy triplets they can be clearly revealed in PL spectra. Our estimate[12] gives about two resonant triplets for a spherical particle of radius 10 nm. The anti-Stokes side of the spectrum is preferable for the observation of the energy quantization because it has a lesser density of the spectral lines. Finally, the giant enhancement provided by fractal aggregates of metal nanoparticles and, especially, by fractal-microcavity composites,[13,14] allowed us to perform our studies of nonlinear PL at low light intensities.

This paper describes a theory and experiments for an unexpected phenomenon in the physics of metal nanoparticles: discrete spectra in the two-photon excited luminescence (TPEL). We interpret this phenomenon as a result of electronic transitions between quantized electronic states in a metal quantum dot. Our preliminary observations of the discrete spectrum for particles of 11 nm in size was reported in Ref. 12. In this paper, experimental results are presented for particles with different mean sizes of 6.5, 11, and 22 nm. A theory of the TPEL from metal quantum dots is developed that successfully interprets a variety of different experiments we performed. Numerical simulations are conducted for multilevel systems representing a single particle and an ensemble of particles with distribution over different sizes as in our experiments.

A theory is developed in the spherical quantum-well model, with an optical response described as a sum of single-particle excitations induced by a plasmon-enhanced local field. The same approach was used, for example, in Refs. 4 and 5 to address the problem of nonlinear susceptibility. The model of degenerated electron gas in an infinite potential well, which we employ in this paper, has proven to be appropriate for many physical problems.[7,15]

The energy E_{nl} for states with quantum numbers nl in a spherical particle of radius R is given by $E_{nl}=E_0\alpha_{nl}^2$, where $E_0=\hbar^2/2mR^2$ and α_{nl} are the $(n+1)$ zeros of the first-kind Bessel functions of the half-integer, $l+1/2$, order.[5] In a particle of radius 10 nm, a characteristic separation between the excited levels, $\delta_F=2(E_FE_0)^{1/2}$, is about 740 cm^{-1} near the Fermi energy E_F; note that this energy spacing is greater than the relaxation width Γ (<100 cm^{-1}).

The intensity spectral density for spontaneous emission at frequency ω_e we find as a sum over all possible transitions $m-l$:

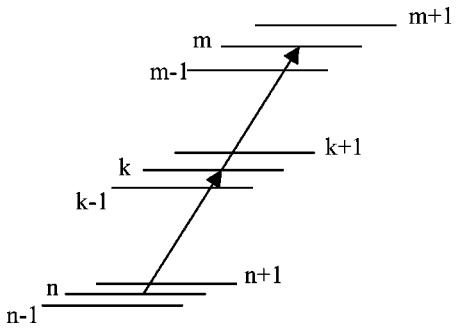

FIG. 1. Sketch of electron transitions in two-photon excitation.

$$I_{sp}=\sum \hbar\omega_{ml}A_{ml}g_m\rho_{mm}(1-\rho_{ll})J(\omega_e,\omega_{ml},\Gamma_2), \quad (1)$$

where $A_{ml}=4\omega_{ml}^3|d_{ml}|^2/(3\hbar c^3 g_m)$ is the Einstein coefficient, ω_{ml} is the $m-l$ transition frequency, and d_{ml} is the dipole reduced matrix element.[16] Factor $g_m=2(2l_m+1)$ in Eq. (1) is the statistical weight for level m and $g_m\rho_{mm}$ is the level population; $(1-\rho_{ll})$ represents the probability to find the lower level unoccupied. Finally, $J(\omega_e,\omega_{ml},\Gamma_2)$ is the spectral profile governed by coherence relaxation rate Γ_2, which is assumed to have a Lorentzian form. Solutions to the density matrix equations can be expressed in the Fourier series form as $\rho_{ij}=\Sigma_{s=-\infty}^{\infty}\rho_{ij}^{(s)}\exp(i\omega st)$, with $\rho_{ij}^{(s)}=(\rho_{ji}^{(-s)})^*$. A system of equations for amplitudes $\rho_{ij}^{(s)}$ in the relaxation constant model has the following form:[5,17]

$$\rho_{ij}^{(s)}=\delta_{s0}\delta_{ij}L_{ij}^{(s)}\Gamma_i N_i+iL_{ij}^{(s)}\sum_p [\mathbb{G}_{ip}(\rho_{pj}^{(s-1)}+\rho_{pj}^{(s+1)}) -(\rho_{ip}^{(s-1)}+\rho_{ip}^{(s+1)})\mathbb{G}_{pj}], \quad (2)$$

where $L_{ij}^{(s)}=[\Gamma_{ij}+i(\omega_{ij}+s\omega)]^{-1}$, $\Gamma_{ii}=\Gamma_i$ is the i state relaxation rate, Γ_{ij} is the coherence relaxation rate for the $i-j$ transition, ω is the field frequency, and N_i is the population of state $i=(n_i,l_i,M_i)$ in the absence of the field. Following Ref. 5 here we use notations: $\mathbb{G}_{ij}=\mathbf{d}_{ij}\mathbf{E}/(2\hbar)$, and $d_{ij}=4eR\alpha_i\alpha_j\sqrt{l_{\max}^{ij}}\delta_{l_i l_j\pm1}/(\alpha_i^2-\alpha_j^2)^2$ where $l_{\max}^{ij}=\max[l_i,l_j]$ (Ref. 16); $\hat{\mathbf{d}}$ and $\mathbf{E}$ are the dipole moment and electric field vectors, respectively.

In this paper, we do not consider polarization effects and focus on the emission spectra and their discreteness. In this case, one can use the averaged over M matrix element G_{ij} that can be defined as $|G_{ij}|^2=(2l_i+1)^{-1}\Sigma_{M_jM_iM_i'}\mathbb{G}_{ij}\mathbb{G}_{ji}$. It gives $|G_{ij}|^2=(12\hbar l_i)^{-1}|d_{ij}|^2|E|^2$, where $l_i\gg1$ and linear polarization is assumed.[5] The strongest effect of the field occurs for transitions with the maximal $\mathrm{Re}\,L_{ij}^{(-s)}|d_{ij}|^2$. Thus, the resonant transitions and transitions with minimal energies provide the largest contributions and must be taken into consideration. We also take into account that $\Gamma_{ij}\ll\omega_{ij}$, ω, and $\omega_{ij}-s\omega\ll\omega$, for resonant frequencies, whereas $\omega_{ij}\ll\omega$, for low frequencies. These two regions do not overlap since $\hbar\omega\gg\delta_F$.

In calculating the electron distribution over energy states, we consider a set of three-level systems providing the largest resonant contributions to two-photon excited PL (the probability to also have three-photon resonance simultaneously with one- and two-photon resonances is negligible). A sketch of the levels involved is shown in Fig. 1, where levels m, k, and n ($E_m>E_k>E_n$) are the resonant levels, whereas others describe the off-resonant neighbor states. The density matrix equations for such system of levels are derived from Eq. (2) and they are as follows:

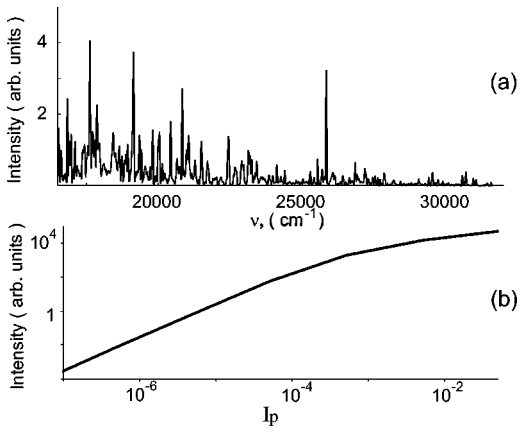

FIG. 2. (a) Calculated spectra for two-photon excited luminescence: $\Gamma_1=5$ cm^{-1}, $\Gamma_2=20$ cm^{-1}, $\lambda_p=632$ nm, particle radius $R=10$ nm. (b) Emission intensity vs dimensionless pump intensity $I_p=|E|^2(eR/\hbar\omega)^2$.

$$\Gamma_m\rho_{mm}^{(0)}=2\,\mathrm{Im}(\rho_{mk}^{(-1)}G_{km})-f_{mm\pm1},$$

$$\Gamma_k\rho_{kk}^{(0)}=\Gamma_k N_k+2\,\mathrm{Im}(\rho_{kn}^{(-1)}G_{nk}-G_{km}\rho_{mk}^{(-1)})-f_{kk\pm1},$$

$$\Gamma_n\rho_{nn}^{(0)}=\Gamma_n N_n-2\,\mathrm{Im}(G_{nk}\rho_{kn}^{(-1)})-f_{nn\pm1},$$

$$\rho_{mk}^{(-1)}=iL_{mk}^{(-1)}[G_{mk}(\rho_{kk}^{(0)}-\rho_{mm}^{(0)})-\rho_{mn}^{(-2)}G_{nk}],$$

$$\rho_{kn}^{(-1)}=iL_{kn}^{(-1)}[G_{kn}(\rho_{nn}^{(0)}-\rho_{kk}^{(0)})+G_{km}\rho_{mn}^{(-2)}],$$

$$\rho_{mn}^{(-2)}=iL_{mn}^{(-2)}[G_{mk}\rho_{kn}^{(-1)}-\rho_{mk}^{(-1)}G_{kn}],$$

$$f_{jj\pm1}=(4\Gamma_{pj}/\omega^2)[|G_{jj-1}|^2(\rho_{jj}^{(0)}-\rho_{j-1j-1}^{(0)}) -|G_{j+1j}|^2(\rho_{j+1j+1}^{(0)}-\rho_{jj}^{(0)})]. \quad (3)$$

We set population $N_j=0$ for $E_j>E_F$, and $N_j=1$ for $E_j<E_F$. The $m\pm1$ notation implies the upper and lower levels nearest to m involved in the allowed transitions; the same is used for k and n. The terms $f_{jj\pm1}$ reflect spreading of level population over neighbor levels. System (3) should be added by recurrent series of equations for $\rho_{j+1j+1}^{(0)}$ expressed in terms of $\rho_{j+2j+2}^{(0)}$ and $\rho_{jj}^{(0)}$, and so on: $\Gamma_p\rho_{pp}^{(0)}=\Gamma_p N_p-f_{pp\pm1}$. The number of such levels involved depends on the field E. In our simulations we set $\rho_{m\pm5}^{(0)}$ to be equal to $N_{m\pm5}$ to "close" system (3). It provides a good approximation for the intensity range used in our experiments. System (3) is solved numerically for each level k from the region $E_F-\hbar\omega<E_k<E_F+\hbar\omega$, with n and m chosen from the resonant triplet states. Note that such a procedure covers a whole set of one-photon, two-photon, and double (one-photon plus

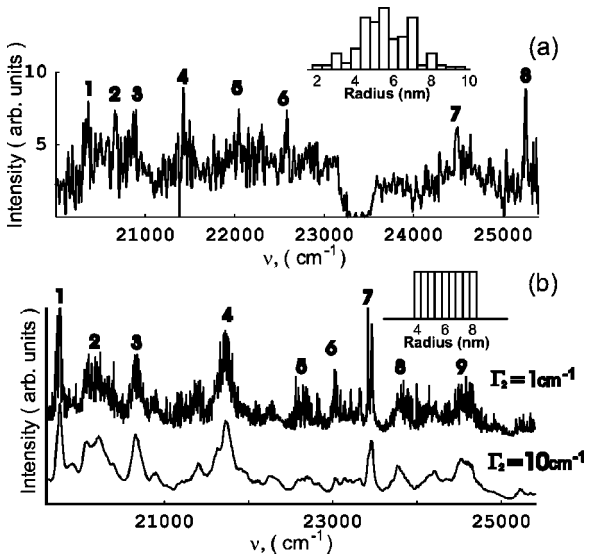

FIG. 3. (a) Experimental emission spectrum obtained with Ag(PVP) colloid at 632 nm, 4-ns pulse excitation. For detection, a 1800-gr/mm grating with 8-cm^{-1} resolution at 2.5×10^4 cm^{-1} was used. (The dip around 23000 cm^{-1} is caused by backside peak of the notch filter.) Inset: particle size distribution. (b) Calculated spectra: $\lambda_p=632$ nm, $I_p=0.03$, ''square'' size-distribution for particles radii, $R=4-8$ nm; upper spectrum, $\Gamma_1=0.5$ cm^{-1}, $\Gamma_2=1$ cm^{-1}; lower spectrum, $\Gamma_1=5$ cm^{-1}, $\Gamma_2=10$ cm^{-1}.

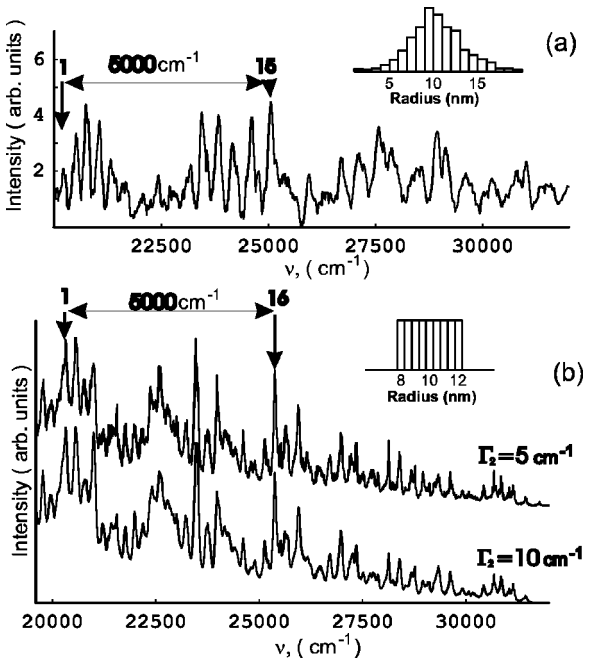

FIG. 4. Experimental emission spectrum obtained with Ag(LM) colloid aggregates in microcavity at 632 nm, cw He-Ne laser excitation; for detection, a 300 gr/mm grating was used. Inset: particle size distribution. (b) Calculated spectra: $\lambda_p=632$ nm, $I_p=0.03$, ''square'' size-distribution for particles radii, $R=8-12$ nm; upper spectrum, $\Gamma_1=5$ cm^{-1}, $\Gamma_2=10$ cm^{-1}; lower spectrum, $\Gamma_1=5$ cm^{-1}, $\Gamma_2=20$ cm^{-1}.

two-photon) resonances. The relaxation constants are assumed the same for all levels and transitions $\Gamma_i=\Gamma_1$ and $\Gamma_{ij}=\Gamma_2$.

The population relaxation constant Γ_1 is related to the kinetic rate for linear optical response[18,19] and multiphoton electron photoemission[20] under femtosecond excitation. It is measured to be in the range 0.5–2 ps so that $\Gamma_1\sim2.5-10$ cm^{-1}. Sometimes Γ_2 is associated with the conductivity relaxation rate, i.e., $2\Gamma_2\sim\gamma_\infty=v_F/l_\infty=140$ cm^{-1}, where l_∞ is the bulk mean free path.[6] Strictly speaking, Γ_2 describes the spectral lines' half-width for transitions between discrete electron states, and it has not been measured directly. We consider Γ_2 as a fitting parameter for experimental spectra; it is found that the minimal spectral line width is 20–40 cm^{-1}. It gives an upper limit for $2\Gamma_2$ since the lines can be broadened due to the particle size distribution.

Our numerical simulations based on the described theory show the discrete spectra for particles with the radius up to 30 nm. The density of spectral lines increases with the particle size, light intensity, and the degree of dispersion in the size distribution. Figure 2(a) shows calculated spectra for monodisperse 10-nm particles. It is interesting to note that despite the enormous number of possible transitions (exceeding 10^4) the discreteness of electron energy states clearly manifests itself, because of the discussed resonant selectivity in multiphoton PL. Moreover, the spectrum remains discrete even when particles have different sizes, as shown in Figs. 3(b) and 4(b) where distributions in ranges 4–8 and 8–12 nm were assumed. The spectral peaks are somewhat broadened with respect to the case of monodisperse 10-nm particles. The density of spectral lines becomes less for particle sizes of 4–8 nm [Fig. 3(b)]. The calculated intensity dependence [Fig. 2(b)] shows the expected quadratic dependence, for relatively low intensities, and then it saturates. Note that the local-field frequency dependence can influence the spectral envelope; this effect will be discussed elsewhere. The emission intensity per electron in a particle can be estimated from Eq. (1) as $\hbar\omega_{ml}A_{ml}\approx3.6\times10^{-13}E_F^2R^{-2}$ W, where E_F is expressed in eV and R in nm.

We observed discrete spectra in two-photon PL in two different sets of experiments, using (i) a high-power ns-pulse excitation of colloid aggregates and (ii) a cw low-power excitation of aggregates in microcavities, where particularly strong enhancement of optical responses occurs.[12,13] Experiments were conducted with Ag colloid aggregates of two types. The first of them, Ag(PVP),[21] was prepared using EtOH solution of polyvinylpyrrolidone (PVP) and NaOH. The second type [Ag(LM)] was prepared by using the Lee-Meisel method,[22] involving the reduction of silver nitrate by an aqueous solution of sodium citrate in concentrations 5×10^{-4} M and followed by aggregation promoted with NaCl. Transmission electron microscopy indicates the mean particle radius $R_0\sim6.5$ nm in the first case and $\sim$ 11 nm for the second one. Radiation from samples in both cases is collected at 90° to incident radiation and sent to Acton imaging spectrograph with a CCD detector. To avoid possible spectral contamination a laser bandpass and notch filters were used. Composite spectra were obtained by superimposing several overlapping spectral regions using long-or short-wavelength pass filters placed after the sample to isolate each region.

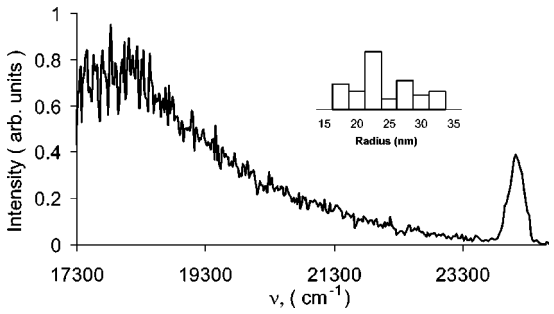

FIG. 5. Experimental emission spectrum obtained with Ag(LM) colloid aggregates at 831 nm, 3 ps TiSph laser excitation of 250-MW/cm^2 intensity. Inset: particle size distribution for particle mean radii of about 22 nm.

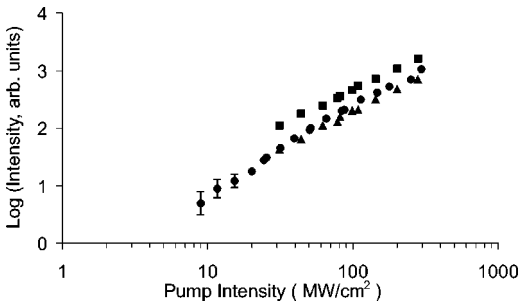

FIG. 6. Intensity dependences for two-photon luminescence (triangles: $\lambda_p = 831$ nm; circles: $\lambda_p = 748$ nm) and hyper-Rayleigh scattering (squares: $\lambda_p = 831$ nm).

This procedure eliminates possible spectral contamination by grating ghosts or overlapping diffraction orders.

The Ag(PVP) aggregated particles are irradiated by 4-ns optical parametric oscillator (MOPO) pulses at $\lambda_L = 632$ nm with a beam focused into a square-cross-section 1×1-cm cuvette. The intensity of the excitation at the cuvette is estimated as $I \approx 300-500$ MW/cm^2. The path length of the emitted light in the colloid is approximately 1–1.5 mm. We note that the intensity used is close to the breakdown threshold of ethanol, which is about 1.5–2 GW/cm^2.[23] For light intensity above 1.5 GW/cm^2, we observed a continuouslike broad spectrum in the range 500–800 nm centered at the pump wavelength from EtOH(PVP) solution. To eliminate the ethanol breakdown, measurements are performed below the threshold, where no emission from the EtOH(PVP) solution is observed. We detected discrete spectra for anti-Stokes emission from Ag (PVP) aggregates in the 330–630-nm range, as shown in Fig. 3(a) (the measured particle size distribution in our samples is shown in the inset). Note that this spectrum, which we attribute to colloidal Ag particles, is qualitatively different from the spectrum observed from the solvent at higher intensities. A comparison of major lines shows a good agreement with the calculated spectrum shown in Fig. 3(b). The average distance $\Delta\nu_{av}$ between major peaks (enumerated in Fig. 3) is about 640 cm^{-1} for measured spectrum and 650 cm^{-1} for the calculated spectrum. The average spectral width of the major lines $\delta\nu$ is about 40–60 cm^{-1}. The close value of spectral width in the calculated spectrum is obtained at the fitting parameter $\Gamma_2 = 1$ cm^{-1} which indicates a broadening of spectral lines due to an overlapping at high density of lines for each particle and for size distribution.

A low-power cw He-Ne pump laser at $\lambda_L = 632$ nm is used for the second type of experiments. Instead of a single path cuvette, Ag(LM) aggregates are seeded into a microcavity, consisting of a hollow quartz tube of outer diameter of 1 mm and inner diameter of 0.7 mm. A laser beam is focused near the inner rim of the tube in a plane perpendicular to its axis with a beam diameter of about 50 μm. The estimated light intensity is about 200 W/cm^2. The spectra obtained are extremely broad, spanning a range from at least 200 to 800 nm. The spectrum on the anti-Stokes side shown in Fig. 4(a) consists of several groups of well-resolved lines. In the ω to 2ω region, the spectral resolution is from 5 to 20 cm^{-1}. Spectral intervals between lines are much greater than spectral features of the microcavity modes which have equidistant spacing of about 2 and 13 cm^{-1}.[12] The intensity dependence of the anti-Stokes emission shows an initially nonlinear behavior and then saturation, in accordance with our simulations. The average interval $\Delta\nu_{av} \approx 360$ cm^{-1} is close to 370 cm^{-1} for calculated spectra [Fig. 4(b)]. The width $\delta\nu$ is about 150 cm^{-1} for the experiment, which is close to the calculated 130 cm^{-1} at $\Gamma_2 = 10$ cm^{-1} and to 170 cm^{-1} at $\Gamma_2 = 20$ cm^{-1}.

Now we compare our results for particle mean sizes of 6.5 and 11 nm. The measured ratio of the average intervals is $\Delta\nu_{av}(6.5\text{ nm})/\Delta\nu_{av}(11\text{ nm}) \approx 1.8$. Since the characteristic interval is $\sim E_0^{1/2} \sim 1/R$ the estimated ratio is about 1.7. The measured ratio for the spectral widths is about $\delta\nu(11\text{ nm})/\delta\nu(6.5\text{ nm}) \approx 3$. Since the spectral lines are broadened the spectral width should be proportional to the number of states in a characteristic interval, which is $\sim R^2$. It gives the estimate for the widths ratio as 2.8. Thus we conclude that the experimental discrete spectra shown in Figs. 3(a) and 4(a) are both in accord with theoretical calculations shown in Fig. 3(b) and 4(b), and demonstrate the expected size dependence. The observed spectral lines are narrow and indicate that there is no diffuse scattering from the particle surface. Our experiments with larger particles, specifically with Ag(LM) colloids of mean size $R = 22$ nm, show that the spectra become continuous-like in this case. In these experiments, we used 750–850 nm, 3 ps pulses of a TiSph laser, and photomultiplier tube (PMT) detection with photon counting. A representative spectrum at a pump wavelength of 831 nm is shown in Fig. 5 along with the particle size distribution (inset). The spectrum contains a broad luminescence band and a peak of hyper-Rayleigh scattering at the second harmonic. The particle shape is more complicated here as compared to the case of small particles. That could be a reason why the second harmonic (SH) becomes allowed.[24] The spectra for large particles and their aggregates are similar to those reported in Ref. 10 for metal rough surfaces. The resolution for the shown spectrum is about 4 nm (130 cm^{-1} at 550 nm). A gradual decrease of the resolution to 0.14 nm results in a corresponding decrease of the broad band intensity, while the narrow SH peak intensity does not change. The spectral width of the SH peak (full width at the half height) is determined by the resolution until it approaches a low limit of about 0.3 nm at a resolution about 0.14 nm. The

low limit in our case can be estimated as half of the laser spectral width, which is about 0.4 nm measured at 0.07-nm resolution. The nonquadratic intensity dependences shown in Fig. 6 illustrate the saturation effect for both two-photon luminescence and the second harmonic. The slope of the curves in the log-log scale becomes approximately 1.3 at the pump intensity above 30 Mw/cm^2.

We also performed time-resolved measurements with PMT detection. A pulse duration of anti-Stokes emission from Ag(PVP) colloid excited with Nd:YAG (yttrium aluminum garnet) laser (14 ns, 1064 nm) was about 10 μs. This indicates that the observed emission is PL, rather than scattering. The model of relaxation constants assumes the population relaxation time $\sim\Gamma_1^{-1}$ which is taken to be the same for all states. The upper limit for the emission time can be estimated from Eq. (1) as $A_{ml}^{-1}=4$ μs for $R=7$ nm. The measured emission time is close to A_{ml}^{-1} but much greater than Γ_1^{-1}. This suggests a need for a more detailed study of population relaxation kinetics, which may have specific features in the discrete multilevel system obeying Pauli's exclusion principle. This problem will be discussed elsewhere. In conclusion, a detailed analysis of the observed discrete spectra and a qualitative agreement with the developed theory allow us to attribute the observed spectra to transitions between the quantized energy states of electrons in metal nanoparticles.

This work was supported in part by NSF Grant No. DMR-0071901, NASA Grant No. NCC-1-01049, and RFBR-02-02-17785.

[1] A. Kawabata and R. Kubo, J. Phys. Soc. Jpn. **21**, 1765 (1966).
[2] L. P. Gor'kov and G. M. Eliashberg, Zh. Eksp. Teor. Fiz. **48**, 1407 (1965) [Sov. Phys. JETP **21**, 940 (1965)].
[3] U. Kreibig, J. Phys. F: Met. Phys. **4**, 999 (1974).
[4] F. Hache, C. Ricard, and C. Flytzanis, J. Opt. Soc. Am. B **3**, 1647 (1986).
[5] S. G. Rautian, Zh. Eksp. Teor. Fiz. **112**, 836 (1997) [Sov. Phys. JETP **85**, 451 (1997)].
[6] U. Kreibig and M. Volmer, *Optical Properties of Metal Clusters* (Springer-Verlag, Berlin, 1995).
[7] W. P. Halperin, Rev. Mod. Phys. **58**, 533 (1986).
[8] R. Kubo, in *Polarization, Matie're et Rayonnement* (Press University de France, Paris, 1969).
[9] J. Lambe and S. L. McCarthy, Phys. Rev. Lett. **37**, 923 (1976).
[10] C. K. Chen, A. R. B. de Castro, and Y. R. Shen, Phys. Rev. Lett. **46**, 145 (1981).
[11] B. N. J. Persson and A. Baratoff, Phys. Rev. Lett. **68**, 3224 (1992).
[12] V. P. Drachev, W. Kim, V. P. Safonov, V. A. Podolskiy, N. S. Zakovryazhin, V. M. Shalaev, and R. A. Armstrong, J. Mod. Opt. **49**, 645 (2002).
[13] W. Kim, V. P. Safonov, V. M. Shalaev, and R. L. Armstrong, Phys. Rev. Lett. **82**, 4811 (1999).
[14] V. M. Shalaev, *Nonlinear Optics of Random Media: Fractal Composites and Metal-Dielectric Films* (Springer, Berlin, 2000).
[15] D. M. Wood and N. W. Ashcroft, Phys. Rev. B **25**, 6255 (1982).
[16] I. I. Sobelman, *Introduction to the Theory of Atomic Spectra* (Pergamon, Oxford, 1973).
[17] S. G. Rautian and A. M. Shalagin, *Kinetic Problems of Nonlinear Spectroscopy* (North-Holland, Amsterdam, 1991).
[18] R. N. M. Groeneveld, R. Sprik, and A. Lagendijk, Phys. Rev. B **51**, 11433 (1995).
[19] N. Del Fatti, R. Bouffanais, F. Vallee, and C. Flytzanis, Phys. Rev. Lett. **81**, 922 (1998).
[20] J. Lehmann, M. Merschdorf, W. Pfeiffer, A. Thon, S. Voll, and G. Gerber, J. Chem. Phys. **112**, 5428 (2000).
[21] H. Hirai, J Macromol. Sci-Chem. A **13**, 633 (1979).
[22] P. C. Lee and D. Meisel, J. Phys. Chem. **86**, 3391 (1982).
[23] R. G. Pinnick, P. Chylek, M. Jarzembski, E. Creegan, V. Srivastava, G. Fernandez, J. D. Pendleton, and A. Biswas, Appl. Opt. **27**, 987 (1988).
[24] O. A. Aksipetrov, P. V. Elyutin, A. A. Nikulin, and E. A. Ostrovskaya, Phys. Rev. B **51**, 17591 (1995).